© 2014. Published by The Company of Biologists Ltd | Journal of Cell Science (2014) 127, 4518–4530 doi:10.1242/jcs.156109

RESEARCH ARTICLE

KIF13B regulates angiogenesis through Golgi to plasma membrane trafficking of VEGFR2

Kaori H. Yamada[1,2], Yuki Nakajima[1,2], Melissa Geyer[1,2], Kishore K. Wary[1,2], Masuko Ushio-Fukai[1], Yulia Komarova[1,2] and Asrar B. Malik[1,2,*]

ABSTRACT

Although the trafficking of newly synthesized VEGFR2 to the plasma membrane is a key determinant of angiogenesis, the molecular mechanisms of Golgi to plasma membrane trafficking are unknown. Here, we have identified a key role of the kinesin family plus-end molecular motor KIF13B in delivering VEGFR2 cargo from the Golgi to the endothelial cell surface. KIF13B is shown to interact directly with VEGFR2 on microtubules. We also observed that overexpression of truncated versions of KIF13B containing the binding domains that interact with VEGFR2 inhibited VEGF-induced capillary tube formation. KIF13B depletion prevented VEGF-mediated endothelial migration, capillary tube formation and neovascularization in mice. Impairment in trafficking induced by knockdown of *KIF13B* shunted VEGFR2 towards the lysosomal degradation pathway. Thus, KIF13B is an essential molecular motor required for the trafficking of VEGFR2 from the Golgi, and its delivery to the endothelial cell surface mediates angiogenesis.

KEY WORDS: VEGFR2, Angiogenesis, Kinesin, Signal transduction, Trafficking

INTRODUCTION

The binding of vascular endothelial growth factor (VEGF) to the endothelial-cell-membrane-bound high-affinity receptor tyrosine kinase VEGFR2 plays a principal role in angiogenesis (Shibuya and Claesson-Welsh, 2006; Ferrara, 2009). Impaired angiogenesis is a feature of ischemic diseases of multiple organs, whereas excessive vascularity contributes to the pathogenesis of inflammatory diseases, cancers and retinal vasculopathies (Folkman, 2007; Potente et al., 2011). Human VEGF receptors (VEGFRs) are composed of an extracellular domain with seven immunoglobulin-like repeats, a transmembrane domain and an intracellular kinase domain that is separated into two segments by a tyrosine kinase insert (Matsumoto and Claesson-Welsh, 2001; Shibuya and Claesson-Welsh, 2006; Nagy et al., 2007). Binding of the $VEGF^{165}$ isoform to VEGFR2 induces the formation of the VEGFR2–neuropilin complex, leading subsequently to VEGFR2 homodimerization and autophosphorylation at multiple tyrosine sites (Matsumoto and Claesson-Welsh, 2001; Shibuya and Claesson-Welsh, 2006; Nagy et al., 2007). The phosphorylated receptor thus becomes a coded template for the recruitment of adaptor and signaling proteins (Shibuya and Claesson-Welsh, 2006; Bruns et al., 2009). VEGFR2 phosphorylation at Y1175 recruits high-affinity substrates such as PLCγ, which activates the MAPK pathway, among others, and Shb, which activates phosphoinositide 3-kinase (PI3K)–Akt pathways (Nagy et al., 2007; Sakurai et al., 2005). Upon internalization post-activation, a portion of the 'spent' VEGFR2 is ubiquitylated and degraded in lysosomes, whereas another portion is recycled to the plasma membrane for another round of activation (Ewan et al., 2006; Singh et al., 2007). In addition, the newly synthesized VEGFR2 is trafficked from the Golgi apparatus to the plasma membrane where it can be activated (Gampel et al., 2006; Manickam et al., 2011). The delivery of VEGFR2 to the endothelial plasma membrane thus appears to be an important limiting mechanism in angiogenesis. The evidence for this is, in part, based on findings showing, for example, that inhibition of trafficking prevents VEGF-mediated neo-vascularization in the ears of mice (Manickam et al., 2011). However, the molecular details of this important process are not well understood. We previously demonstrated that the kinesin-3 protein, KIF13B, was important for the growth of neurites and establishment of neuronal polarity (Horiguchi et al., 2006). Because common signaling pathways regulate both vascular and axonal growth, and multiple parallels exist between the two processes (Herbert and Stainier, 2011), an attractive hypothesis is that KIF13B mediates angiogenesis through trafficking of VEGFR2 to its proper destination at the endothelial plasma membrane. Based on our preliminary studies demonstrating that KIF13B is prominently expressed in endothelial cells, here, we have studied the role of KIF13B in the trafficking of VEGFR2 from its site of synthesis to the endothelial plasma membrane. We demonstrate the kinetics of KIF13B-mediated VEGFR2 transport from the Golgi to plasma membrane and highlight the role of KIF13B in mediating angiogenesis through the positioning of VEGFR2 at the endothelial cell surface, thus allowing the interaction of VEGFR2 with VEGF.

RESULTS

VEGF activates KIF13B motor function in endothelial cells

First, we used a knockdown approach to test the role of KIF13B in endothelial cells. Human umbilical vein endothelial cells (HUVECs) were infected with lentivirus particles encoding a short hairpin RNA (shRNA) targeting human *KIF13B*. We observed reduced expression of KIF13B in shRNA-treated cells, but not of its closest homolog, KIF13A (Fig. 1A). Endothelial cell sprouting was tested in these cells by three-dimensional (3D) culture of HUVECs on beads (Nakatsu and Hughes, 2008). Control cells exhibited long sprouts and multiple branching

[1]Department of Pharmacology, University of Illinois College of Medicine, Chicago, IL 60612, USA. [2]Center of Lung and Vascular Biology, University of Illinois College of Medicine, Chicago, IL 60612, USA.

*Author for correspondence (abmalik@uic.edu)

Received 6 May 2014; Accepted 31 July 2014

Journal of Cell Science

Journal of Cell Science (2014) 127, 4518–4530 doi:10.1242/jcs.156109

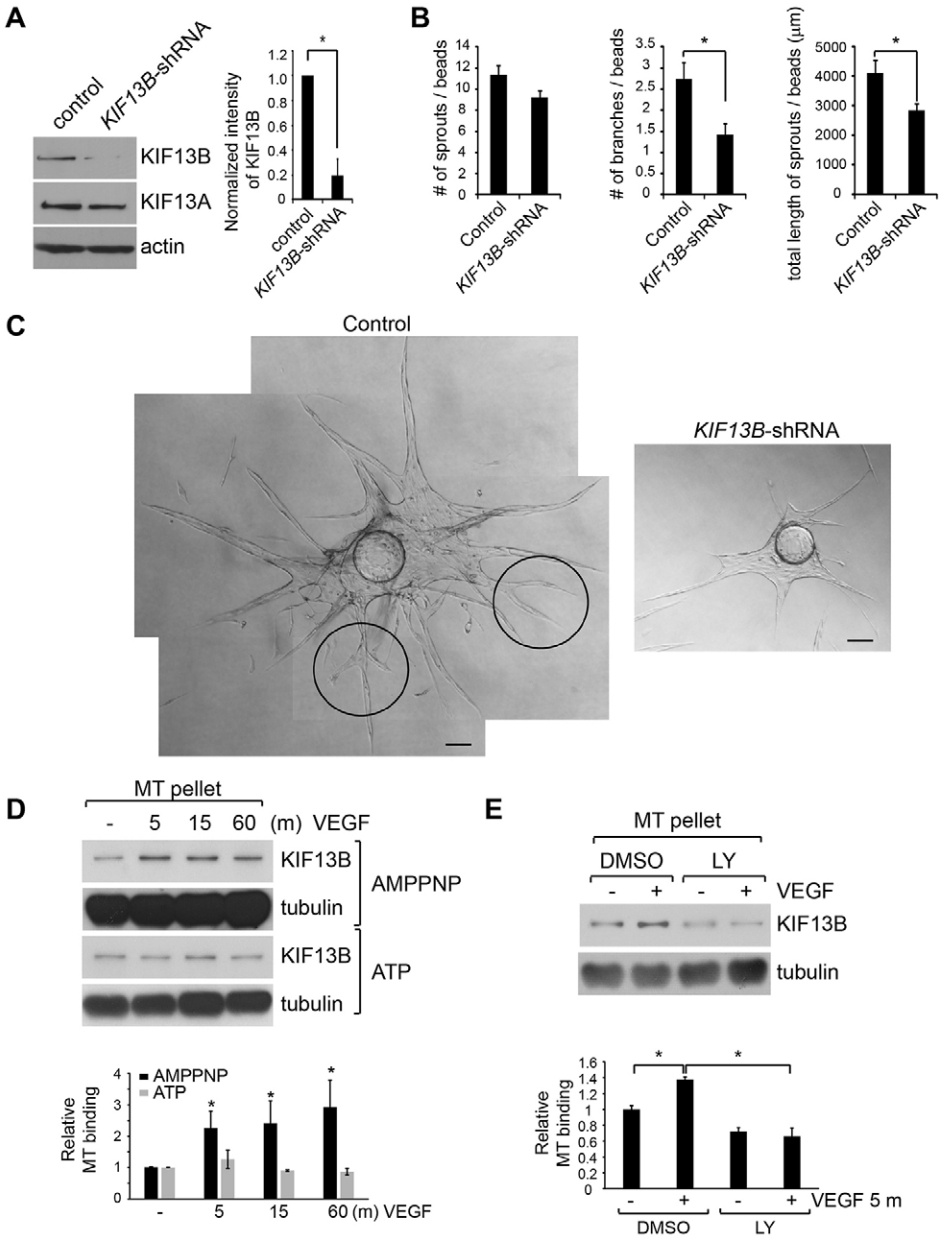

Fig. 1. KIF13B is required for the formation of endothelial tubes and branching point structures through KIF13B binding to microtubules after VEGF stimulation. (A) Left, expression of KIF13B was determined by western blotting in extracts of HUVECs treated with either control virus or virus encoding *KIF13B*-shRNA. Densitometric quantification shows knockdown of KIF13B with the shRNA. Right, data show the mean±s.e.m. (n=4); *P<0.05 (two-tailed Student's t-test, P=0.0014). (B,C) *In vitro* 3D sprouting assay in fibrin gel. HUVECs were treated with either control virus or virus encoding *KIF13B*-specific shRNA as indicated. (B) The number of branches and total length of sprouts per bead are shown as the mean±s.e.m. (n=22); *P<0.05 (two-tailed Student's t-test, P=0.066, 0.010, 0.015). (C) Circles indicate branch formations. Scale bars: 100 μm. (D) Microtubule (MT) binding of KIF13B in HUVECs after VEGF stimulation. HUVECs were stimulated with 2.2 nmol/l VEGF for the indicated times (min), and lysates were incubated with 0.1 mg/ml of tubulin, 20 μM taxol and 2.5 mM AMPPNP, the hydrolysis-resistant ATP analog (Verhey et al., 1998), or ATP. Proteins bound to microtubules were precipitated by ultracentrifugation and analyzed by western blotting. Densitometric quantification shows that VEGF induced microtubule binding of KIF13B. Microtubule binding of KIF13B was augmented by the presence of AMPPNP in contrast to ATP. Data are shown as the mean±s.e.m. (n=3); *P<0.05 (one-way ANOVA, F=3.0, F critical=2.5). (E) Effect of the PI3K inhibitor LY294002 (LY) on the microtubule binding of KIF13B in HUVECs after VEGF stimulation. HUVECs were pre-incubated with DMSO or LY294002 (25 μM) and stimulated with 2.2 nmol/l VEGF for 5 min. The microtubule binding assay was performed as described above. Densitometric quantification shows inhibition of VEGF-induced microtubule binding of KIF13B by the PI3K inhibitor; data show the mean±s.e.m. (n=3); *P<0.05 (one-way ANOVA, Bonferroni multiple comparisons test, F=25.8, F critical=6.6).

points, whereas *KIF13B*-knockdown cells showed reduced sprout lengths and fewer branching points (Fig. 1B,C).

We next addressed whether VEGF, the VEGFR2 ligand, was itself capable of stimulating the motor activity of KIF13B. Intracellular transport function of kinesins is regulated by three interrelated mechanisms; (1) binding of kinesins to the cargo, (2) binding of kinesins to microtubules and (3) activation of the ATPase function of kinesins (Hirokawa et al., 2009; Morfini et al., 2009). The ATP-bound form of the motor domain of kinesins binds to microtubules and the motor is released from microtubules after ATP hydrolysis (Verhey et al., 1998). To test this overall concept, we performed the microtubule binding assay in the presence of AMPPNP, a hydrolysis-resistant ATP analog (Verhey et al., 1998). We observed that VEGF promoted microtubule binding of KIF13B in the presence of AMPPNP, but not ATP (Fig. 1D). We also determined the effect of the PI3K inhibitor LY294002 on the microtubule binding of KIF13B, because VEGF signaling is known to activate PI3K (Graupera et al., 2008). PI3K inhibition prevented the VEGF-induced microtubule binding of KIF13B (Fig. 1E), suggesting that VEGF functions through PI3K-dependent binding of KIF13B to microtubules.

KIF13B binding to VEGFR2 at the Golgi initiates VEGFR2 trafficking

We next determined whether KIF13B was capable of binding to the VEGFR2 cargo, a prerequisite for its function in transporting VEGFR2. Our studies demonstrated that VEGFR2 co-immunoprecipitated with KIF13B in a time-dependent manner following stimulation of HUVECs with VEGF (Fig. 2A). Increased co-immunoprecipitation of VEGFR2 with KIF13B was evident from 5 min after the onset of VEGF stimulation, increasing to 5.5±0.9-fold (±s.e.m.) above baseline at 1 h (n=5 experiments, P<0.05) and remaining elevated up to 240 min (Fig. 2A). We also observed by Optiprep gradient separation that VEGFR2 was present in the low-density plasma membrane,

Journal of Cell Science (2014) 127, 4518–4530 doi:10.1242/jcs.156109

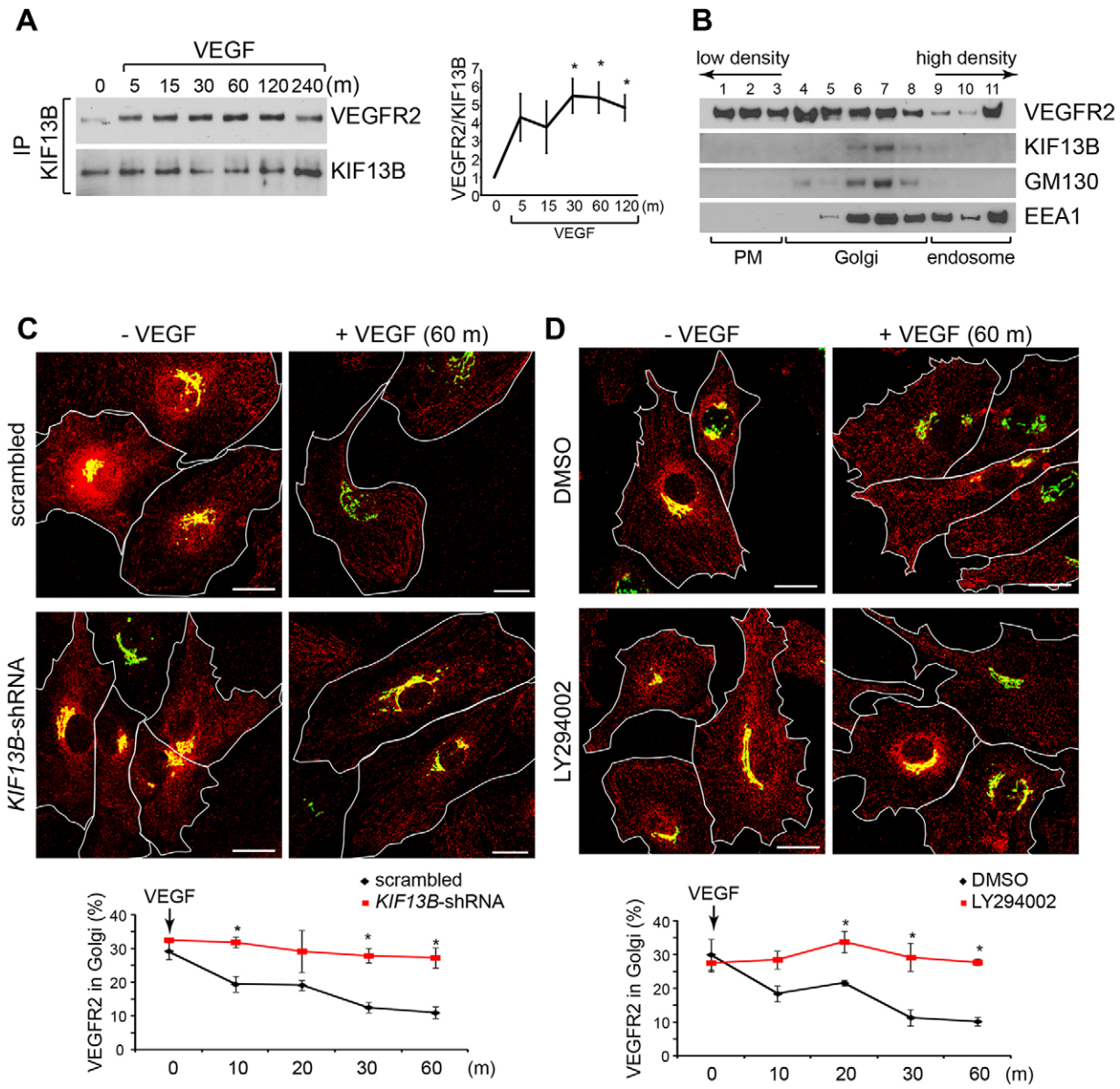

Fig. 2. VEGF signaling induces the association of VEGFR2 with KIF13B in the Golgi. (A) Co-immunoprecipitation of VEGFR2 with immunoprecipitated (IP) KIF13B in HUVECs following stimulation with VEGF (2.2 nmol/l). VEGF stimulation induces VEGFR2 interaction with KIF13B within 5 min, and this interaction increased during the 240-min period of study. The ratio of VEGFR2:KIF13B is shown (right panel) as the mean±s.e.m. (*n* values are 5, 3, 3, 3, 5 and 3 for 0, 5, 15, 30, 60 and 120 min, respectively); **P*<0.05 (one-way ANOVA, Bonferroni multiple comparisons test, *F*=5.05, F critical=2.85). (B) Subcellular fractionation of serum-starved HUVECs. Homogenates prepared from HUVECs were fractionated on an Optiprep gradient (10%, 20% and 30%) and immunoblotted with antibodies against proteins enriched in the Golgi (GM130) and endosomes (EEA1). VEGFR2 and KIF13B were detected using specific antibodies. Results are representative of three experiments and show the association of VEGFR2 with KIF13B in Golgi. PM, plasma membrane. (C) Upper panel, immunostaining of VEGFR2 (red) and GM130 (green) in HUVECs treated with scrambled shRNA or *KIF13B*-specific shRNA lentivirus and stimulated with 2.2 nmol/l VEGF for 1 h. KIF13B deletion reduces VEGFR2 release from the Golgi. White lines indicate cell outlines. Lower panel, the percentage of VEGFR2 that colocalized with GM130 was quantified and is shown as the mean±s.e.m. (*n*=5); **P*<0.01 (one-way ANOVA, Bonferroni multiple comparisons test, *F*=13.1, F critical=2.14). (D) Upper panel, immunostaining of VEGFR2 (red) and GM130 (green), a Golgi marker, in HUVECs treated with 2.2 nmol/l VEGF for 1 h in the presence or absence of the PI3K inhibitor LY294002 (25 μM). Scale bars: 20 μm. LY294002 prevented the release of VEGFR2 from Golgi. Lower panel, the percentage of VEGFR2 that colocalized with GM130 was quantified and is shown as the mean±s.e.m. (*n*=4); **P*<0.05 (one-way ANOVA, Bonferroni multiple comparisons test, *F*=6.2, F critical=2.2).

Golgi and endosome fractions, whereas KIF13B was present primarily in the Golgi fraction along with the Golgi marker GM130 (also known as GOLGA2), with little KIF13B evident in the endosomes (Fig. 2B), suggesting that KIF13B interacted with VEGFR2 primarily in the Golgi. Furthermore, we observed by immunostaining that, basally, ∼30% of VEGFR2 was localized in the Golgi before VEGF stimulation as reported previously (Manickam et al., 2011), whereas VEGF signaling itself was responsible for initiating the transport of VEGFR2 away from the Golgi (Fig. 2C). We used a knockdown approach to test the role of KIF13B in mediating VEGFR2 transport. In control cells we observed a strong baseline localization of VEGFR2 in the Golgi, which decreased during the 60 min period after VEGF stimulation (Fig. 2C), consistent with VEGFR2 trafficking out

Journal of Cell Science (2014) 127, 4518–4530 doi:10.1242/jcs.156109

of the Golgi. KIF13B-depleted cells, however, showed persistent VEGFR2 localization in the Golgi (Fig. 2C). Inhibition of the release of VEGFR2 was also confirmed by subcellular fractionation (supplementary material Fig. S1A,B). As PI3K regulates the binding of KIF13B to microtubules (Fig. 1E), we also examined the role of PI3K in VEGFR2 trafficking by using the PI3K inhibitor LY294002 (Fig. 2D). We observed that LY294002 prevented VEGFR2 release from the Golgi (Fig. 2D), suggesting that PI3K regulates KIF13B-mediated transport of VEGFR2 from the Golgi following VEGF stimulation. However, LY294002 did not affect KIF13B binding to VEGFR2 (supplementary material Fig. S1C).

KIF13B is required for processive anterograde VEGFR2 trafficking

We next determined whether the interaction of KIF13B with VEGFR2 could support directionality of VEGFR2 trafficking. To quantify VEGFR2 trafficking from the Golgi to the plasma membrane, we carried out time-lapse microscopy of vesicles that were double positive for GFP and mCherry following the expression of VEGFR2–GFP and mCherry–KIF13B in HUVECs (Fig. 3A; supplementary material Movies 1, 2). Exogenously expressed VEGFR2–GFP and mCherry–KIF13B were primarily colocalized in vesicular structures around the nuclei of HUVECs. Colocalization of exogenously expressed VEGFR2–GFP and mCherry–KIF13B was evident before VEGF stimulation (supplementary material Movie 1) and remained unchanged after VEGF stimulation (supplementary material Movie 2). Before VEGF stimulation, most of the vesicles were undergoing either random slow short-range movements or were stationary (supplementary material Movie 1). After stimulation with VEGF, GFP and mCherry double-positive vesicles showed directional movement towards the cell periphery (anterograde direction) and to some extent towards the perinuclear area (retrograde direction) (Fig. 3A; supplementary material Movie 2).

To examine the role of KIF13B in VEGFR2 movement, we expressed VEGFR2–GFP in KIF13B-depleted HUVECs. VEGF signaling activated both fast and long-range transport in scrambled-shRNA-treated controls, in contrast to virtually no movement in KIF13B-depleted cells (Fig. 3B–D). Examples of vesicle movement are shown in Fig. 3B, and kymograph recordings are shown in Fig. 3C (upper panel). The results are shown as histograms of vesicle velocity (Fig. 3D) and lengths of movement (Fig. 3C, lower panel). The mean velocity of anterograde movement of VEGFR2-positive vesicles in control cells was 0.10±0.005 μm/s (±s.e.m.) before VEGF stimulation, and this increased to 0.16±0.01 μm/s, 0.26±0.01 μm/s and 0.34±0.03 μm/s at 5 min, 15 min and 30 min, respectively, after VEGF stimulation (Fig. 3D, left). This increase was caused by an increase in the number of vesicles with faster velocities over time, as opposed to each vesicle speeding up over time (Fig. 3D, left). KIF13B depletion prevented the increase in velocity primarily in the anterograde direction (Fig. 3D, right; from 0.07±0.002 μm/s before treatment with VEGF to 0.09±0.007 μm/s, 0.09±0.003 μm/s and 0.13±0.005 μm/s at 5 min, 15 min and 30 min, respectively, after VEGF stimulation). The mean length of anterograde movement was also increased by VEGF stimulation (Fig. 3C, lower panel; 0.15±0.01 μm before VEGF treatment to 0.30±0.05 μm, 0.55±0.11 μm and 0.62±0.10 μm at 5 min, 15 min and 30 min, respectively, after VEGF stimulation). However, this was not seen in KIF13B-depleted cells (Fig. 3C, lower panel; 0.11±0.006 μm before treatment with VEGF to 0.14±0.02 μm, 0.13±0.006 μm/s and 0.21±0.02 μm at 5 min, 15 min and 30 min, respectively, after VEGF stimulation). These results show the essential role of KIF13B in the anterograde transport of VEGFR2 in endothelial cells.

KIF13B regulates the localization of VEGFR2 at the endothelial cell surface

We next used biotinylation of cell surface proteins and immunostaining to determine whether KIF13B mediated the localization of VEGFR2 at the endothelial cell surface. In these studies, HUVECs were treated with lentivirus carrying either scrambled control shRNA or *KIF13B*-specific shRNA, and were subsequently stimulated with VEGF (Fig. 4A). Cell surface proteins were labeled with biotin, and VEGFR2 on the cell surface was detected by western blotting of streptavidin precipitates. Basal VEGFR2 cell surface expression was similar in control and KIF13B-depleted cells (Fig. 4A). VEGF stimulation markedly decreased VEGFR2 cell surface localization (Fig. 4A), indicating receptor internalization. However, the cell surface expression of VEGFR2 was restored to ∼70% of basal level within 8 h in control cells, but only to ∼25% in *KIF13B*-knockdown cells (Fig. 4A). The restoration of the cell surface positioning of VEGFR2 was confirmed by immunostaining cell surface VEGFR2 using an antibody against the extracellular domain (Fig. 4B,C). Before VEGF stimulation, similar amounts of VEGFR2 were seen at the plasma membrane of both control and KIF13B-depleted cells, consistent with the cell surface biotin-labeling data reported above (Fig. 4A). Cell surface levels of VEGFR2 decreased significantly at 1 h after VEGF stimulation under both conditions but were restored at the cell surface within 4–8 h only in controls (Fig. 4B,C). Neither VEGF treatment nor *KIF13B* depletion led to significant changes in microtubule dynamics or organization of the microtubule cytoskeleton as assessed by high-throughput analysis of EB1–GFP tracks and immunofluorescent staining for both acetylated and tyrosinated tubulin (supplementary material Fig. S4). Taken together, these findings demonstrate that the effect of knocking down KIF13B is the result of impaired VEGFR2 transport on microtubule tracks.

KIF13B-mediated cell surface localization of VEGFR2 is required for receptor activation

We next determined whether the KIF13B-mediated positioning of VEGFR2 at the cell surface (Fig. 4A–C) is necessary for receptor activation. We observed that VEGF stimulation induced the phosphorylation of VEGFR2 within 5 min in both control and KIF13B-depleted cells (Fig. 4D). Control cells displayed a decrease in both VEGFR2 expression and phosphorylation, both of which were progressively restored within 8 h after VEGF stimulation (Fig. 4D). However, VEGFR2 phosphorylation and protein expression were both markedly reduced in KIF13B-depleted cells after VEGF stimulation compared with that of control cells, and VEGFR2 expression failed to recover in these cells (Fig. 4D).

Because VEGFR2 is degraded after internalization (Ewan et al., 2006; Rahimi, 2009), *de novo* synthesis is required to replenish the lost cell surface pool (Domingues et al., 2011). Thus, we next investigated the *de novo* synthesis of VEGFR2 by real-time polymerase chain reaction (RT-PCR). Depletion of KIF13B did not interfere with VEGFR2 synthesis (data not shown), it only impaired the transport of the receptor to the plasma membrane as shown above (Fig. 4A–C).

Journal of Cell Science (2014) 127, 4518–4530 doi:10.1242/jcs.156109

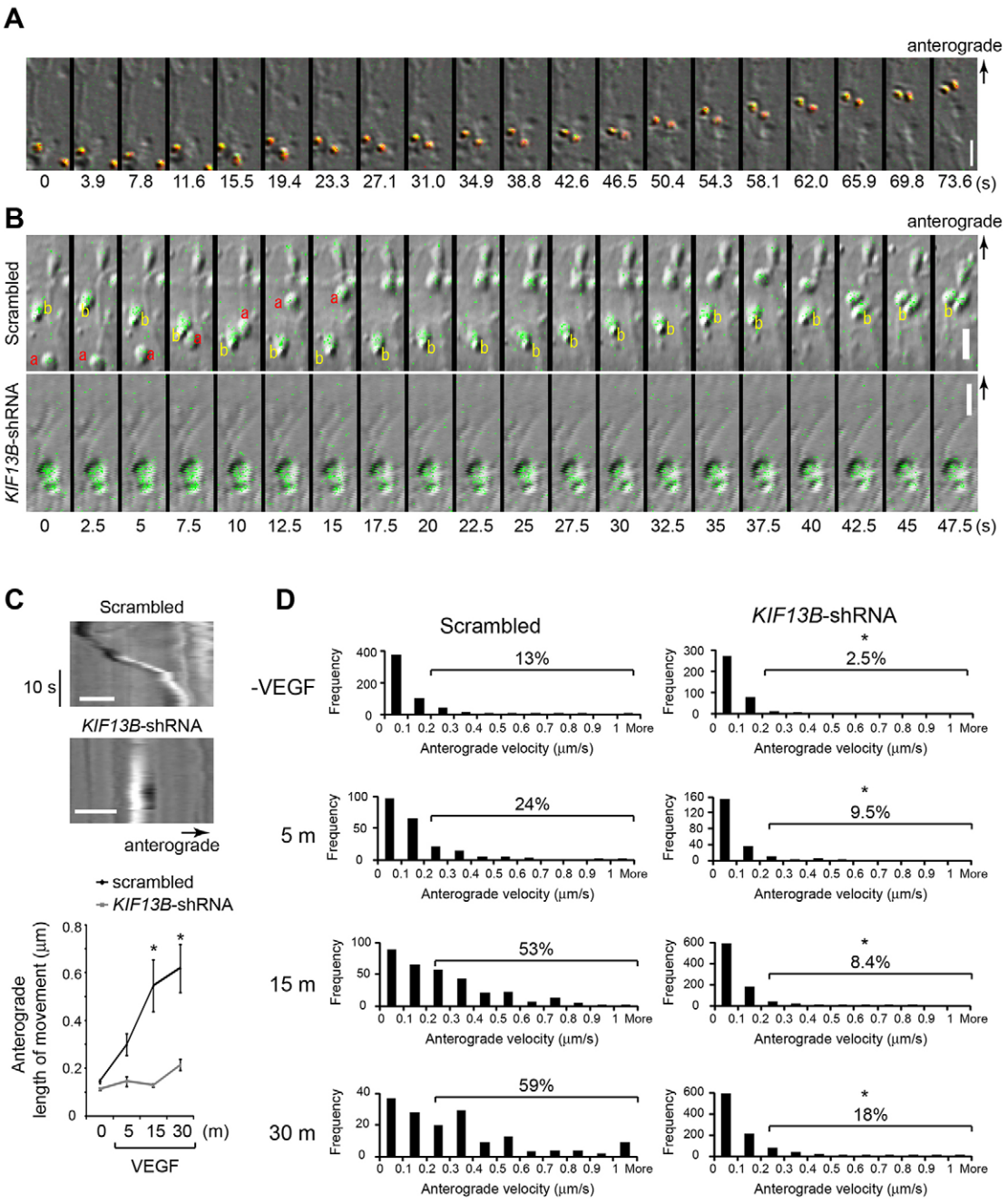

Fig. 3. KIF13B is required for the processive anterograde transport of VEGFR2. (A) Sequential micrographs taken over a 73.6-s period showing the directional movement of vesicles positive for VEGFR2–GFP (green) and mCherry-KIF13B (red) (merged image in yellow) towards the plasma membrane (anterograde direction, arrows) in HUVECs stimulated with 2.2 nmol/l VEGF. The total distance travelled was 6 μm. Scale bar: 2 μm. (B) Sequential micrographs taken over a 47.5-s period in scrambled-shRNA-treated control and *KIF13B*-depleted HUVECs. VEGFR2–GFP-positive vesicles moved processively in the anterograde direction towards the plasma membrane in control HUVECs stimulated with 2.2 nmol/l VEGF. Distances travelled by vesicles a and b were 5.1 and 3.7 μm, respectively. By contrast, processive movement of VEGFR2–GFP-positive vesicles was not observed in HUVECs treated with *KIF13B*-specific shRNA. Scale bars: 2 μm. (C) Upper panel, kymographs showing tracks of vesicles in scrambled-shRNA-treated control and *KIF13B*-depleted HUVECs. Scale bars: 2 μm. Lower panel, graphs showing the lengths of movement of VEGFR2-positive cells as determined by kymograph before VEGF treatment and at 5, 15 and 30 min after VEGF stimulation. Experiments were repeated four times. Sequential pictures were taken over 50 s in a single movie to observe vesicles in two cells. We took 15 movies altogether for each condition in each experiment. Then, 5–10 vesicles in each movie were tracked using Metamorph to measure the velocity and length of movements. Length of movements was measured for vesicles continuously moving in the anterograde direction. The data show the mean±s.e.m.; **P*<0.01 (one-way ANOVA, Bonferroni multiple comparisons test, $F=22.2$, F critical=2.02). (D) Histograms showing the anterograde processive velocity of VEGFR2–GFP-positive vesicles in HUVECs treated with either scrambled shRNA or *KIF13B*-specific shRNA. VEGF stimulation increased the number of vesicles showing processive movement in control cells, whereas this was not seen in *KIF13B*-depleted HUVECs. **P*<0.01 (one-way ANOVA, $F=103.7$, F critical=2.01).

Journal of Cell Science (2014) 127, 4518–4530 doi:10.1242/jcs.156109

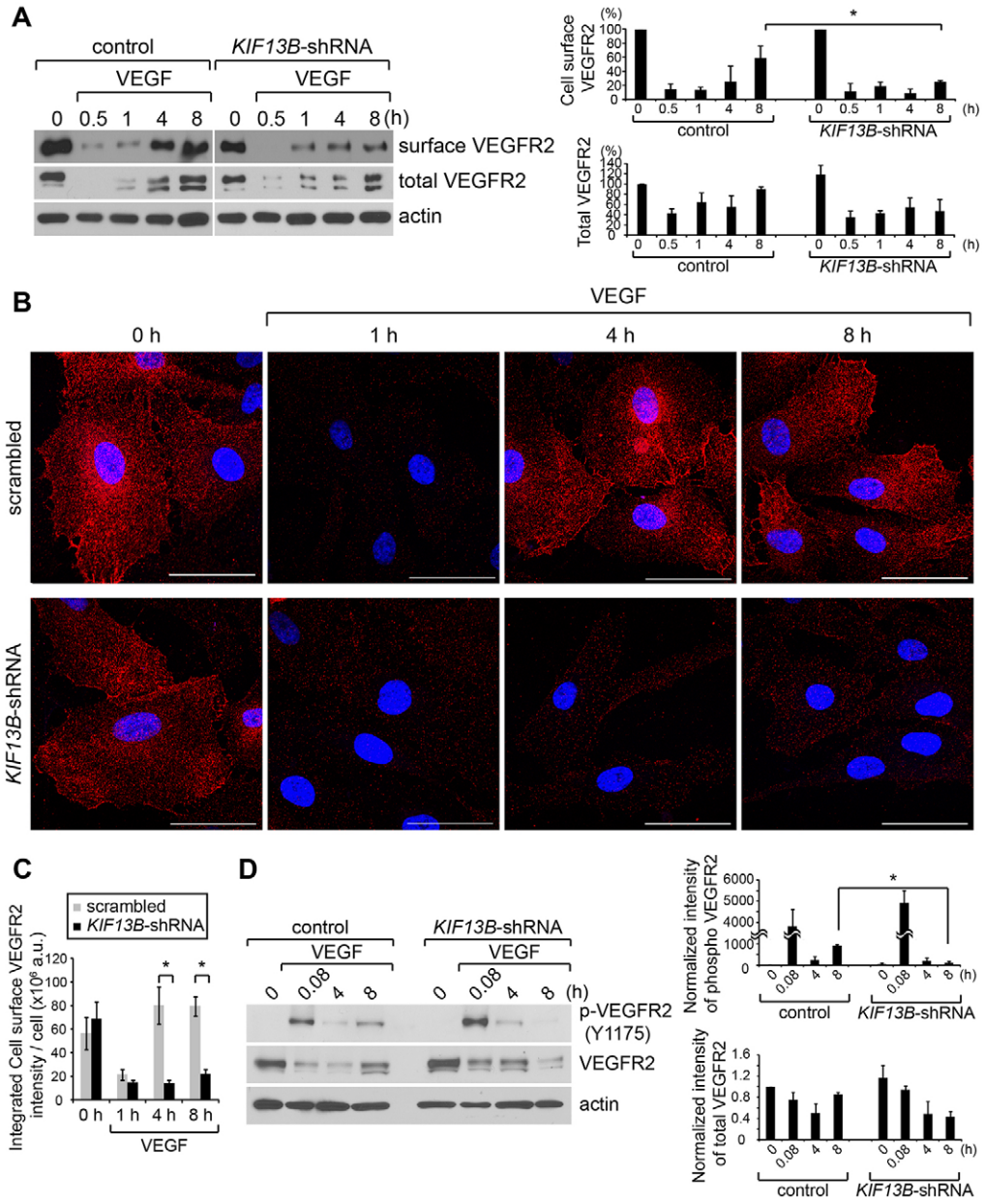

Fig. 4. KIF13B is required for endothelial cell surface positioning of VEGFR2. (A) Assessment by biotin labeling of cell-surface-localized VEGFR2, showing the timecourse of return of VEGFR2 to the cell surface after VEGF stimulation. HUVECs treated with either control shRNA or *KIF13B*-specific shRNA were stimulated with VEGF (2.2 nmol/l) for the indicated times. Cell surface proteins were labeled with biotin and collected using streptavidin beads. Left, VEGFR2 at the cell surface and in the total cell lysate was detected using specific antibody. Right, densitometric quantification of the timecourse of return of cell surface VEGFR2 post-VEGF stimulation was performed. Cell surface VEGFR2 was normalized to the basal amount of cell surface VEGFR2. Quantified total VEGFR2 is also shown. $n=3$; *$P<0.05$ (one-way ANOVA, Bonferroni multiple comparisons test; cell surface, $F=9.67$, F critical=3.14; total, $F=3.29$, F critical=2.22). (B) Timecourse of plasmalemmal localization of VEGFR2 after VEGF (2.2 nmol/l) treatment of HUVECs as determined by immunofluorescent staining with antibody against the extracellular domains of VEGFR2 (red). Nuclei are shown in blue. VEGF treatment induced depletion of cell surface VEGFR2 at 1 h post-VEGF stimulation, and this was restored by 4 h. Scale bars: 50 μm. (C) Quantification of cell surface expression of VEGFR2. Cell surface VEGFR2 is expressed as the integrated intensity of the threshold area in each cell. a.u., arbitrary units. Data show the mean±s.e.m. ($n=19, 16, 8, 14, 16, 19, 21$ and 14); *$P<0.05$ (one-way ANOVA, $F=7.86$, F critical=2.09). (D) Phosphorylation of VEGFR2 at Y1175 in response to VEGF (2.2 nmol/l) stimulation of HUVECs treated with either control shRNA or *KIF13B*-specific shRNA. Left, cell extracts were probed for phosphorylated Y1175, total VEGFR2 and actin immediately at the onset of VEGF stimulation (0.08 h) and at 4 and 8 h after VEGF stimulation when VEGFR2 cell surface expression had been restored (Fig. 4A). Results show impaired VEGFR2 phosphorylation in *KIF13B*-depleted endothelial cells compared with that of control cells. KIF13B-mediated transport of VEGFR2 to the plasma membrane is required for VEGFR2 activation. Right, densitometric quantification of VEGFR2 phosphorylation and degradation (normalized to actin) is shown in upper and lower graphs, respectively, as the mean±s.e.m. ($n=4, 4, 3$ and 3); *$P<0.05$ (one-way ANOVA, phosphorylated VEGFR2, $F=24.6$, F critical=2.5; total VEGFR2, $F=3.22$, F critical=2.5).

Journal of Cell Science (2014) 127, 4518–4530 doi:10.1242/jcs.156109

Impaired KIF13B motor function shunts VEGFR2 to lysosomes

We next studied whether KIF13B-mediated transport of VEGFR2 to the plasmalemma was coupled to VEGFR2 avoidance of the lysosomal degradation pathway. HUVECs pretreated with either scrambled shRNA or *KIF13B*-specific shRNA were pre-incubated with DMSO or bafilomycin A1 (Baf), an inhibitor of vacuolar-type H^+-ATPase (Ewan et al., 2006), for 1 h, and then exposed to VEGF for an additional 4 h. The localization of VEGFR2 in lysosomes was examined by immunostaining with antibodies against VEGFR2 and LAMP2, a lysosomal marker (Eskelinen et al., 2003). In scrambled-shRNA-treated controls, treatment with Baf increased the colocalization of VEGFR2 with LAMP2 from 9.6±1.1% to 36.4±1.4% (±s.e.m.) (supplementary material Fig. S2), indicating that a portion of VEGFR2 was localized in lysosomes after receptor internalization. However, in *KIF13B*-shRNA-treated cells, VEGFR2 accumulated in lysosomes, particularly in large perinuclear lysosomes (58.4±3.3%), whereas DMSO-treated control cells showed only 16.1±2.0% colocalization (supplementary material Fig. S2), indicating a default pathway for VEGFR2 translocation to lysosomes following KIF13B depletion.

KIF13B-mediated VEGFR2 cell surface localization regulates endothelial cell migration, tubulogenesis and vessel formation

Based on the above observations showing the required role of KIF13B in mediating the transport of VEGFR2 to the plasma membrane (Fig. 4), we addressed whether KIF13B is a determinant of endothelial migration and tube formation in culture and *in vivo*. *KIF13B* knockdown significantly reduced VEGF-mediated migration of HUVECs (Fig. 5A). We also used small interfering RNA (siRNA) that was specific for *KIF13B* (supplementary material Fig. S1D) and that targeted a sequence different from that targeted by *KIF13B*-specific shRNA. *KIF13B* knockdown in this study significantly reduced VEGF-mediated migration of HUVECs, whereas scrambled siRNA had no effect (Fig. 5B). *KIF13B*-depleted cells were then subjected to the two-dimensional (2D) tube formation assay. Control cells formed branching point structures, and *KIF13B* knockdown significantly reduced the number of these structures (Fig. 5C,D). Importantly, we were able to rescue the effects of *KIF13B* depletion with shRNA-resistant FLAG–KIF13B (Fig. 5C,D). Expression of KIF13B in *KIF13B*-depleted HUVECs fully restored the tube-forming

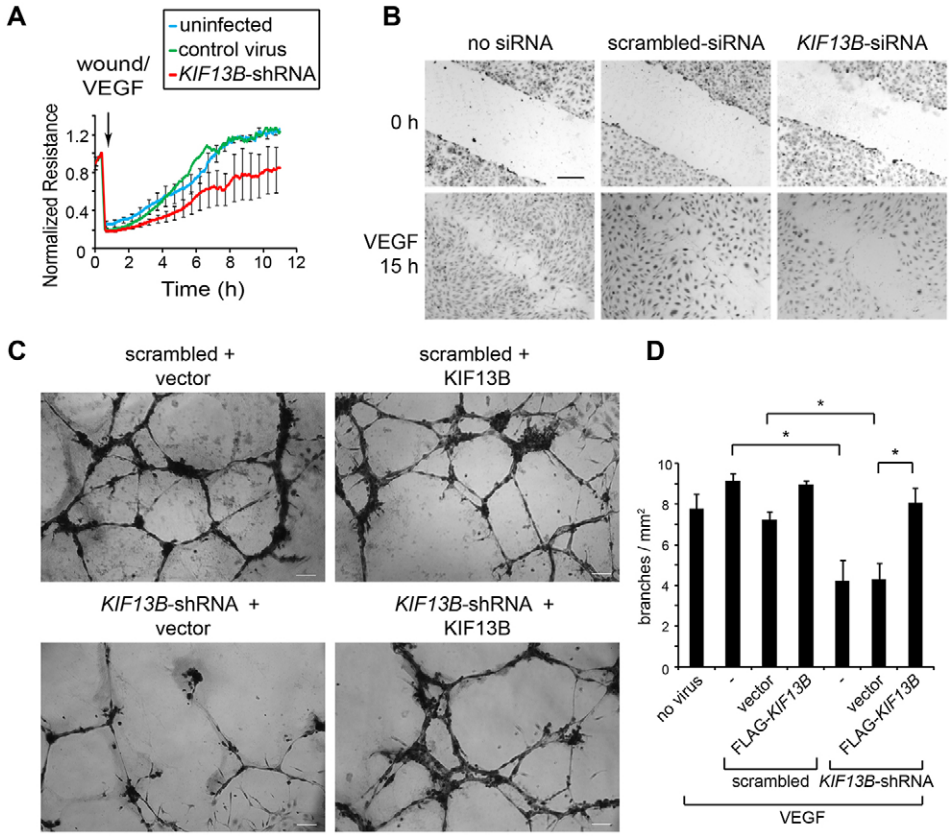

Fig. 5. KIF13B is required for VEGF-mediated endothelial cell migration and capillary-network formation. (A) VEGF-mediated migration of HUVECs was determined by transendothelial electrical resistance (TER) measurements (Keese et al., 2004). A confluent monolayer of HUVECs received an elevated field pulse (2.0 V at 40 kHz for 5 s) and was monitored for recovery in the presence of 2.2 nmol/l VEGF. HUVECs were treated with either control virus or virus encoding *KIF13B*-specific shRNA and were tested in a TER system for cell migration. (B) VEGF-mediated migration of HUVECs was determined by using the scratch wound healing assay (Humtsoe et al., 2010). HUVECs were treated with scrambled control siRNA or *KIF13B*-specific siRNA and were subjected to the scratch wound healing assay in the presence of 2.2 nmol/l VEGF. At the indicated times, cells were fixed and stained with Hematoxylin. Scale bar: 200 μm. (C) *In vitro* 2D capillary-like network formation. HUVECs were treated with either control virus or virus encoding *KIF13B*-specific shRNA and transfected with vector or FLAG–KIF13B. At 2 d thereafter, cells were seeded onto Matrigel in the presence of 2.2 nmol/l VEGF, and fixed and stained with Hematoxylin at 16 h after seeding. Representative images are shown. Scale bar: 100 μm. (D) *In vitro* 2D capillary-like network formation. The number of branches was counted and is presented as the mean±s.e.m. (n=8, 4, 4, 4, 7, 4 and 7); *P<0.05 (one-way ANOVA, Bonferroni multiple comparisons test, F=6.78, F critical=2.30).

Journal of Cell Science (2014) 127, 4518–4530 doi:10.1242/jcs.156109

ability of these cells (Fig. 5C,D; supplementary material Fig. S1E).

Identification of KIF13B domains interacting with VEGFR2

We also carried out studies to identify the binding sites on KIF13B that mediate its interaction with VEGFR2. Immunoprecipitation binding assays were performed using truncated mutants of KIF13B and full-length VEGFR2 expressed in human embryonic kidney (HEK) 293T cells (supplementary material Fig. S3A). As shown in Fig. 6D, KIF13B has a motor domain (amino acids 1–354), Forkhead-associated domain (FHA; amino acids 448–545), membrane-associated guanylate kinase binding stalk domain (MBS; amino acids 638–833), proline-rich domain (amino acids 1532–1645) and Cap-Gly domain (amino acids 1703–1768) (Hanada et al., 2000; Yamada et al., 2007). The regions between these domains are referred to as linkers (L1, L2 and L3). VEGFR2 bound to the KIF13B fragment containing the motor, FHA and MBS domains (amino acids 1–833) and to the fragment containing linker-3 (L3; amino acids 834–1531), which is located between the MBS and the proline-rich domain of KIF13B, whereas vector and a fragment containing the proline-rich domain to the C terminus (pro-CT; amino acids 1528–1826) did not bind to VEGFR2

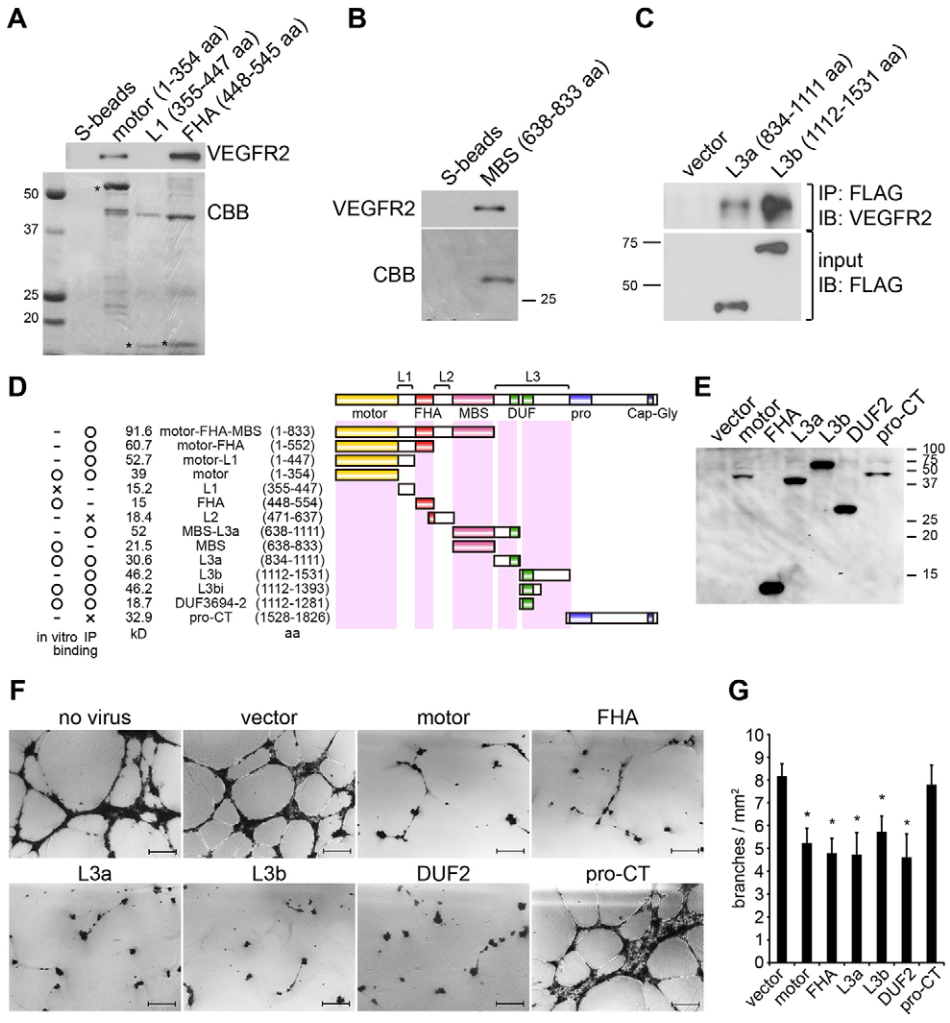

Fig. 6. Identification of the KIF13B domains required for binding to VEGFR2. (A,B) *In vitro* direct binding assay. The KIF13B motor domain [amino acids (aa) 1–354], L1 (amino acids 355–447), FHA domain (amino acids 448–545) and MBS domain (amino acids 638–833) were expressed in bacteria with a His tag and an S tag. Recombinant VEGFR2 (amino acids 790–1356, cytosolic domain, CT) was pulled down by the truncated domains of KIF13B immobilized on S-beads and detected by western blotting using a specific antibody. Truncated KIF13B domains on S-beads were detected by Coomassie Brilliant Blue (CBB) staining. Asterisks show the corresponding truncated mutants, other bands are contaminating proteins from the purification. (C) Co-immunoprecipitation analysis showing the binding site of KIF13B required for interaction with VEGFR2. HEK 293T cells were transfected with GFP–VEGFR2 and truncated mutants of FLAG–KIF13B or control vector. Immunoprecipitation (IP) was performed using FLAG-specific antibody, and VEGFR2 was detected by immunoblotting (IB) with its antibody. VEGFR2 binds to L3a (amino acids 834–1111) and L3b (amino acids 1112–1531). (D) Schematic showing the domains of KIF13B and the truncated versions used in the study. Binding sites are indicated in pink. Dash, not applicable; circle, positive binding; X, no binding. Results are representative of three experiments. (E) Lentivirus-based expression of truncated mutants of KIF13B in HUVECs. HUVECs were infected with lentiviruses encoding truncated mutants of KIF13B or vector. The expressed proteins were detected using an anti-FLAG antibody. (F) *In vitro* 2D capillary-like network formation. HUVECs were treated with either control virus or virus encoding truncated mutants of KIF13B. At 2 d thereafter, cells were seeded on Matrigel in the presence of 2.2 nmol/l VEGF and were fixed and stained with Hematoxylin at 16 h after seeding. Representative images are shown. Scale bars: 200 μm. (G) *In vitro* 2D capillary-like network formation. The number of branches was counted and is presented as the mean±s.e.m. (n=8, 6, 5, 4, 7, 6 and 3); *P<0.05 (one-way ANOVA, Student–Newman–Keuls multiple comparisons test, F=3.73, F critical=2.41).

Journal of Cell Science (2014) 127, 4518–4530 doi:10.1242/jcs.156109

(supplementary material Fig. S3A). To address whether the interaction between KIF13B and VEGFR2 was direct, we expressed recombinant truncated KIF13B in bacteria and determined its ability to pull down recombinant VEGFR2 (amino acids 790–1356, cytosolic domain). The motor, FHA and MBS domains were shown to directly interact with the cytosolic domain of VEGFR2, whereas L1 (355–447 aa) or S-protein agarose (S-beads) alone did not support binding (Fig. 6A,B).

There are two occurrences of the same domain identified within the L3 region of KIF13B from the amino acid sequence similarity on the Pfam database; this domain is termed 'domain of unknown function' (DUF). More than 3000 DUF families are described on the Pfam database. The function of these two DUF domains (DUF3694) in KIF13B is not known. Thus, we tested the interaction of DUF3694 domains with the cytosolic domain of VEGFR2 (CTa, amino acids 790–973 and CTb, amino acids 974–1356). Both DUF3694-1 (DUF1; amino acids 990–1111) and DUF3694-2 (DUF2; amino acids 1112–1281) directly interacted with VEGFR2-CTa, which included the juxta-membrane domain and half of the kinase domain (supplementary material Fig. S3C,D; summarized in Fig. 6D). Taken together, these data suggest that VEGFR2 directly interacts with five distinct binding sites in KIF13B – the motor, FHA, MBS, DUF1 and DUF2 domains.

Next, to test the dominant-negative effect of these truncated mutants of KIF13B, we expressed these constructs by using lentivirus vector (see Materials and Methods for details). HUVECs were infected with lentiviruses encoding FLAG–motor, FLAG–FHA, FLAG–L3a, FLA–L3b, FLAG–DUF2 or FLAG–pro-CT, or with lentiviruses carrying empty vector, and the expressed proteins were detected by using an anti-FLAG antibody (Fig. 6E). HUVECs expressing these truncated mutants or vector-infected control HUVECs were tested in the 2D capillary-like network formation assay. Expression of truncated mutants that bound to VEGFR2 significantly reduced network formation, whereas vector-infected control HUVECs formed capillary networks on Matrigel (Fig. 6F,G). Importantly, the expression of pro-CT, which did not bind to VEGFR2, did not prevent network formation (Fig. 6F,G).

KIF13B mediates angiogenesis *in vivo*

To address the role of KIF13B in mediating *in vivo* angiogenesis, we performed the Matrigel plug assay in mice (Yang and Proweller, 2011) using lentivirus that carried shRNA targeting mouse KIF13B (Fig. 7; supplementary material Fig. S1F). Knockdown in primary mouse pulmonary endothelial cells using mouse-*KIF13B*-specific shRNA was confirmed by western blotting (supplementary material Fig. S1F). We also

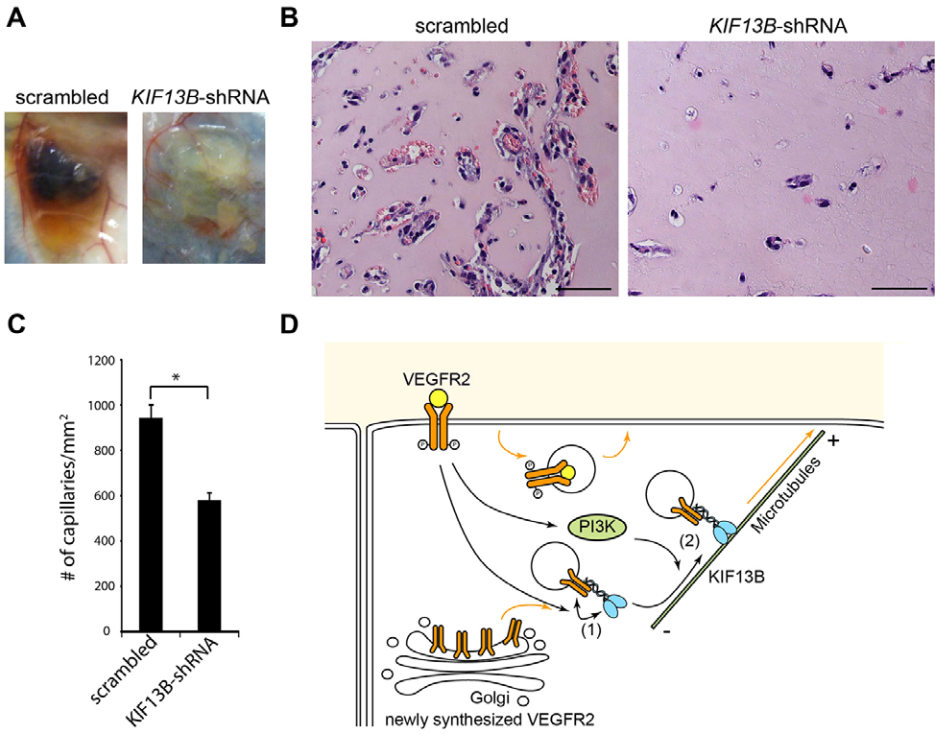

Fig. 7. KIF13B is required for VEGF-mediated angiogenesis and capillary tube formation *in vivo*. (A) Matrigel supplemented with 2.2 nmol/l VEGF, 50 ng/ml bFGF, 60 U heparin and 0.8×10^8 IFU lentivirus (either encoding scrambled shRNA control or *KIF13B*-specific shRNA) was injected subcutaneously into C57BL/6 males. After 4 d, the Matrigel plugs were collected. (B) Hematoxylin and Eosin staining of Matrigel plugs. Scale bars: 50 μm. (C) The number of capillaries per mm^2 is shown as the mean±s.e.m. (n=3 mice and 5 mice for scrambled and *KIF13B*-shRNA, respectively); *P<0.001 (Student's t-test). Five paraffin sections were stained per sample, and 42 and 59 fields were counted for scrambled and *KIF13B*-shRNA groups, respectively. (D) Proposed model describing the fate of VEGFR2 (indicated by orange arrows). VEGF (yellow) induces VEGFR2 internalization and signaling, resulting in a portion of VEGFR2 being degraded. Non-degraded VEGFR2 is recycled back to the plasma membrane. VEGF stimulation also initiates VEGFR2 synthesis and the receptor is transported to the plasma membrane for another cycle of activation. We showed that VEGF induced the release of VEGFR2 from the Golgi (orange arrow) to start transporting to cell surface. This was inhibited by the PI3K inhibitor or by knockdown of KIF13B. (1) VEGF induced direct binding of KIF13B (indicated as blue kinesin dimer) to VEGFR2, independent of PI3K. (2) VEGF also induced binding of KIF13B to microtubules in a PI3K-dependent manner. Thus, direct binding of KIF13B to VEGFR2 on microtubules resulted in vectorial transport of VEGFR2 from the Golgi to endothelial cell surface where it interacts with VEGF and activates the angiogenic program.

confirmed the interaction of KIF13B and VEGFR2 by co-immunoprecipitation analysis in mouse endothelial cells (supplementary material Fig. S1G). A high titer of lentivirus carrying mouse-*KIF13B*-specific shRNA was injected with Matrigel into C57BL mice in the presence of VEGF, bFGF and heparin. In the scrambled-shRNA-treated Matrigel plug, we observed the formation of vessels filled with erythrocytes, whereas *KIF13B* knockdown resulted in a significantly reduced number of vessels (Fig. 7A–C). The vessels observed in *KIF13B*-shRNA-treated Matrigel were smaller and poorly developed. As angiogenesis is also supported by other accessory cells, such as macrophages and fibroblasts (Saharinen et al., 2011), we tested whether KIF13B is expressed in these cells (supplementary material Fig. S1H). KIF13B expression in fibroblasts and macrophages was modest, in contrast to that of endothelial cells.

DISCUSSION

The binding of VEGF to VEGFR2 localized on the endothelial cell surface activates signaling pathways mediating angiogenesis (Matsumoto and Claesson-Welsh, 2001; Shibuya and Claesson-Welsh, 2006). VEGFR2 is internalized upon activation (Gampel et al., 2006; Lanahan et al., 2010), but a portion of the receptor is directed to lysosomes for degradation (Ewan et al., 2006; Singh et al., 2007). The cell surface pool of VEGFR2 is homeostatically replenished by both *de novo* protein synthesis induced by VEGF signaling itself (Gampel et al., 2006; Domingues et al., 2011) and by recycling of residual intact receptor. The process of transport of VEGFR2 to the membrane is essential for sprouting endothelial cells at the tips of growing vessels, where a constant supply of VEGFR2 is needed for vessel outgrowth (Nakayama et al., 2013). In the present study, we demonstrated that the molecular motor kinesin KIF13B is required for the transport and endothelial cell surface positioning of VEGFR2, and hence it was essential for angiogenesis. Using GFP to trace the movement of VEGFR2-loaded vesicles, we observed that depletion of KIF13B reduced both vesicle velocity and processivity in the anterograde direction. Knockdown of *KIF13B* profoundly reduced the ability of endothelial cells to migrate and form tubes and branches in new vessels. The few vessels that formed in the absence of KIF13B were of poor quality. Restoration of KIF13B expression renewed the angiogenic potential of endothelial cells, resulting in the formation of functional vessels, thus indicating that KIF13B was both necessary and sufficient for productive angiogenesis.

In the present study, KIF13B-mediated VEGFR2 trafficking to the plasmalemma was seen only following VEGF-mediated activation. KIF13B depletion had no effect on the constitutive transport of VEGFR2-containing vesicles, indicating that basal trafficking of VEGFR2 occurring in the absence of VEGF stimulation is KIF13B-independent. A previous study showed that the trans-Golgi SNARE protein syntaxin-6 contributed to VEGFR2 trafficking from the Golgi (Manickam et al., 2011). Although we did not examine the relationship between syntaxin-6 and KIF13B, it is plausible that both the SNARE machinery and KIF13B function in a mutually exclusive manner at different points of the transport cycle to transport VEGFR2 to the plasmalemma.

The VEGFR2 pool that escaped lysosomal degradation after internalization returned to the plasma membrane by vesicular recycling. Using biotin to label cell surface proteins, we observed that KIF13B did not interact with the internalized VEGFR2, suggesting that KIF13B was only involved in the transport of newly synthesized receptor to the cell surface. Subcellular fractionation studies showed that KIF13B was primarily localized in the Golgi together with newly synthesized VEGFR2 and, importantly, it was absent from endosomes. The non-degraded VEGFR2 is normally recycled from the endosomes to the plasma membrane within a timecourse of ~35 min (20 min for internalization and 15 min for recycling) (Gampel et al., 2006). We estimated from biotin labeling of cell surface proteins that the amount of recycled VEGFR2 appearing at the plasma membrane accounted for only 14% of the receptor at 1 h after VEGF stimulation. Depletion of KIF13B did not affect the amount of recycled VEGFR2, suggesting that the process of delivery of non-degraded VEGFR2 was independent of KIF13B. KIF13B depletion, however, inhibited the VEGF-induced trafficking of VEGFR2 from the Golgi, consistent with an essential role of KIF13B in mediating only the transport of *de novo* synthesized VEGFR2 to the endothelial cell surface for activation by VEGF.

KIF13B binding to the VEGFR2 cargo and microtubules in the Golgi was seen as early as 5 min after VEGF stimulation, whereas the reappearance of VEGFR2 at the plasma membrane was evident at ~4 h after VEGF stimulation, and VEGFR2 levels at the plasma membrane were fully restored by 8 h. We observed that RNA synthesis of VEGFR2 was induced after stimulation with VEGF, with the peak occurring at 2 h (data not shown). The accumulation of VEGFR2 at the plasma membrane is a function of both on-going VEGFR2 synthesis and the Golgi-to-plasmalemmal VEGFR2 transport that is needed to restore the original amount of receptor at the plasma membrane. The interaction of VEGFR2 and KIF13B also increased in the same time-frame and remained elevated up to 4 h tested in this study. Thus, KIF13B interacted with VEGFR2 throughout the process of transporting the VEGFR2 cargo from Golgi to plasma membrane.

VEGF signaling mediated the direct interaction between KIF13B and VEGFR2 as well as KIF13B binding to microtubules, both of which were necessary for activation of the transport machinery. Interestingly, the microtubule binding of KIF13B was blocked by PI3K inhibition. As KIF13B is known to be highly phosphorylated (Hanada et al., 2000), it is possible that PI3K and/or downstream kinases are responsible for phosphorylation of KIF13B and thereby regulate its activity. PI3K might also regulate the activity of KIF13B through other KIF13B-binding proteins, such as centaurin A (CentA) (Horiguchi et al., 2006), an adaptor for PIP3 binding.

Studies were also performed to identify the binding sites on KIF13B that are responsible for its interaction with VEGFR2. These immunoprecipitation studies and *in vitro* direct binding assays employed multiple truncated mutants of KIF13B and full-length or cytosolic domains of VEGFR2. VEGFR2 was shown to bind to the motor, FHA and MBS domains, and to two DUF3694 domains within the L3 domain of KIF13B. Interestingly, truncated mutants of KIF13B containing the binding domains for VEGFR2 functioned in a dominant-negative manner to inhibit the trafficking of VEGFR2 and formation of a 2D capillary network. These findings are consistent with the specificity of KIF13B in mediating VEGFR2 positioning on the endothelial cell surface. The KIF13B domains described as being involved in binding to VEGFR2 differed from those required for transporting PIP3 in neurons (Horiguchi et al., 2006), suggesting the versatility of the KIF13B motor in interacting with cargos in a cell-specific manner. Although neurons and angiogenesis share some common signaling mechanisms, there are also major differences (Herbert and Stainier, 2011). We clearly showed

Journal of Cell Science (2014) 127, 4518–4530 doi:10.1242/jcs.156109

that dominant-negative KIF13B mutants, which did not block PIP3 transport in neurons (Horiguchi et al., 2006), inhibited tube formation in endothelial cells. Thus, the finding in neurons concerning the role of KIF13B cannot be simply extrapolated to endothelial cells.

In addition to the effect of KIF13B depletion in reducing plasma membrane VEGFR2 localization, we observed that KIF13B deficiency promoted the lysosomal localization of VEGFR2. This result is consistent with the finding that inhibition of the t-SNARE protein syntaxin-6, which blocks post-Golgi trafficking of VEGFR2 to the plasma membrane (Manickam et al., 2011), facilitated lysosomal degradation of VEGFR2. Thus, any failure of proper plasmalemmal localization of VEGFR2 mediated by KIF13B might be a crucial mechanism for shunting VEGFR2 to the default lysosomal pathway.

In conclusion, we describe here the essential role of the kinesin molecular motor KIF13B in transporting newly synthesized VEGFR2 to the plasma membrane of endothelial cells and, thus, in restoring the cell surface pool of VEGFR2 (described in Fig. 7D). The vectorial trafficking of VEGFR2 to the plasma membrane by KIF13B is essential for productive angiogenesis *in vivo*. Based on the novel role of KIF13B in the positioning of VEGFR2 at the plasma membrane described in these studies, targeting KIF13B to prevent VEGFR2 replenishment at the endothelial cell surface represents a novel anti-angiogenesis strategy in disease states.

MATERIALS AND METHODS

Antibodies, inhibitors and recombinant proteins

Antibodies against KIF13A, E-tag (Abcam, Cambridge, MA), KIF13B (Novus Biologicals, Littleton, CO), VEGFR2, phosphorylated VEGFR2 (Y1175) (Cell Signaling, Billerica, MA), extracellular domain of VEGFR2 (Fitzgerald, Acton, MA), actin, VEGFR2 (Santa Cruz, CA), LAMP2 (BD, San Jose, CA), FLAG, GST, KIF13B (Sigma, St Louis, MO), acetylated tubulin (Life Technologies, Grand Island, NY) and tyrosinated tubulin (EMD Millipore, Billerica, MA) were used in this study. Secondary antibodies used were horseradish peroxidase (HRP)-conjugated donkey anti-rabbit-IgG, goat anti-mouse-IgG (Jackson Immunologicals, West Grove, PA), Alexa-Fluor-488-conjugated anti-mouse-IgG and Alexa-Fluor-594-conjugated anti-rabbit-IgG (Life Technologies). Inhibitors used in this study included actinomycin D (Sigma), bafilomycin A1 (Sigma) and LY294002 (Calbiochem, San Diego, CA). GST-tagged recombinant VEGFR2 (amino acids 790–1356) was purchased from Biaffin GmbH & Co KG (Germany).

Plasmids and siRNA constructs

Ambion Silence Select Pre-designed siRNA targeting human *KIF13B* (nucleotides 3394–3412) and Silencer Select negative control were purchased from Life Technologies and transfected into cells by using HiPerfect Transfection Reagent (Qiagen, Valencia, CA). Human *KIF13B* cDNA was purchased from Kazusa DNA institute (Japan). To make the full-length and truncated mutants of KIF13B, the corresponding fragments were amplified by PCR and subcloned into pCMV-Flag-tag2B, pmCherry-C1 and pET29a. The inserted fragment was confirmed by sequencing. To make shRNA-resistant full-length *KIF13B*, t249a/a252t (bp) mutations were induced by site-directed mutagenesis (Agilent Technologies, Santa Clara, CA), because the shRNA targeted nucleotides 241–261 of human *KIF13B*. Human *VEGFR2* cDNA was amplified by PCR and inserted into the *Xho*I and *Kpn*I sites of mCherry-N1 and pEGFP-N1 (Clontech, Mountain View, CA).

Cell culture

HUVECs were purchased from Lonza (Walkersville, NJ) and maintained in EGM-2 (Lonza) supplemented with 10% FBS on culture dishes coated with 0.1% gelatin (Sigma). Passage 4–6 was used for experiments. Before stimulation with $VEGF^{165}$, HUVECs were serum starved in EBM-2 (Lonza) supplemented with 0.1% bovine serum albumin (BSA) (Sigma) for 2 h. Recombinant human $VEGF^{165}$ (Miltenyi Biotech, Auburn, CA) was used at 50 ng/ml (2.2 nmol/l). HEK 293T/17 (ATCC) and human fibroblast Detroit 551 (ATCC, Manassas, VA) were maintained in DMEM (Life Technologies) supplemented with 10% FBS. Mouse embryonic fibroblasts (MEFs) and mouse bone-marrow-derived macrophages were isolated and cultured as described previously (Itoh et al., 2008; Zhang et al., 2008; Di et al., 2011).

Lentivirus preparation

To prepare short hairpin RNA (shRNA) lentivirus vector targeting nucleotides 241–261 of *KIF13B*, the forward primer 5′-CCG-GAAAGTGCCTTGGAGAGAATATCCTCGAGGATATTCTCTCCAA-GGCACTTTTTTTTG-3′ and reverse primer 5′-AATTCAAAAAAAAG-TGCCTTGGAGAGAATATCCTCGAGGATATTCTCTCCAAGGCAC-TTT-3′ were synthesized, annealed and inserted into pLKO.1. To express truncated mutants of KIF13B, the corresponding fragments were amplified by PCR and subcloned into pRRL-FLAG-IRES-DsRed vector. 293T/17 cells were transfected with pCMV-dR8.74, pMD1.G VSV-G and one of pLVTH-GFP, pLKO.1-scrambled-shRNA, pLKO.1-*KIF13B*-shRNA, pRRL-FLAG-IRES-DsRed vector, pRRL-FLAG-motor, pRRL-FLAG-FHA, pRRL-FLAG-L3a, pRRL-FLAG-L3b, pRRL-FLAG-DUF2 or pRRL-FLAG-pro-CT, and virus supernatants were collected thereafter. For *in vivo* experiments, lentivirus was concentrated using lentiX-concentrator (Clontech). The titer of the lentivirus was measured by real-time-PCR-based methods with the lentiX-qRT-PCR titration kit (Clontech).

Endothelial cell sprouting assay

To induce sprouting of HUVECs, the fibrin gel sprouting assay was performed as described previously (Nakatsu and Hughes, 2008; Newman et al., 2011). Three components of vessel growth were measured. The mean number of sprouts per bead was determined by counting the number of sprouts. The mean number of branch points per bead represented the number of sprout bifurcations per bead. The mean total length per bead represented the cumulative length of all sprouts per bead. For each condition, 20 beads were assessed and mean values were calculated.

Microtubule binding studies

Microtubule binding was performed as described previously (Verhey et al., 1998) with some modifications. HUVECs were lysed in BRB80 (80 mM PIPES-KOH, 2 mM $MgCl_2$ and 1 mM EGTA) supplemented with 1 mM β-glycerophosphate, 10 mM sodium fluoride, 1 mM sodium orthovanadate and protease inhibitor cocktail (Sigma). After centrifugation at 14,000 ***g*** for 5 min at 4℃, supernatants were further centrifuged at 135,000 ***g*** with the TLA55 rotor (Beckman-Coulter) for 10 min at 4℃. Supernatants were incubated with 2.5 mM ATP or AMP-PNP (Sigma), 0.1 mg/ml of tubulin and 20 µM taxol (Calbiochem) at 30℃ for 30 min to polymerize microtubules, overlaid on a glycerol cushion (BRB80 with 60% glycerol) and centrifuged at 135,000 g with the TLA55 rotor for 10 min at 25℃. Supernatants were removed and pellets were washed once with warm BRB80, dissolved with 2% SDS and analyzed by western blotting.

Subcellular fractionation

Subcellular fractionation was performed using Optiprep as described previously (Manickam et al., 2011).

Image acquisition

Immunostained cells were visualized with a Zeiss confocal LSM 510 META with Apochromat 63× water-immersion objective lens. For the wound healing scratch assay, 2D tube formation assay and fibrin gel sprouting assay, the images were captured with a Zeiss Axiovert 200 M phase-contrast microscope with EC Plan-Neofluar 5× objective lens and AxioCamHS digital camera. To record the formation of capillaries in the Matrigel plug assay, a Zeiss Axiovert phase contrast microscope was used with Plan Neofluar 40× oil-immersion objective lens, and AxioCamMR5 camera. Live imaging for vesicle trafficking was

performed by using a Zeiss LSM710 confocal microscope with 63× oil-immersion objective lens, operated by Zen (Zeiss). Microtubule dynamics were recorded by using a Nikon Eclipse TE-2000S microscope equipped with UltraView confocal head (PerkinElmer Life Sciences, Waltham MA), ORCA-ER-1394 camera (Hamamatsu, Japan), AR/KR three line laser (λ=488, 568 and 647 nm), a Plan Apo 100× 1.4 NA objective and Volocity 5 software (Improvision, PerkinElmer).

Live-cell imaging

For the analysis of vesicle trafficking, HUVECs were transfected with VEGFR2–GFP and mCherry–KIF13B using X-treme GENE HP (Roche). At 1 d after transfection, cells were serum starved in EBM without Phenol Red (Lonza) supplemented with 0.1% BSA for 1 h. Cells were stimulated with 2.2 nmol/l VEGF, and vesicle trafficking was observed before VEGF stimulation (basal) and at 5 min, 15 min and 30 min after VEGF stimulation. To test the effects of *KIF13B* knock down in VEGFR2 trafficking, HUVECs were treated with either scrambled shRNA lentivirus or *KIF13B*-shRNA at a multiplicity of infection of 1. Cells were further transfected with VEGFR2–GFP using X-treme GENE HP (Roche) and tested by live-cell imaging. Images were taken twice per second, and vesicles were tracked by Metamorph (Molecular Devices, Sunnyvale, CA). Processive movement was determined if the movement continued in the same direction for at least two frames. Length of processive movements and the velocity of anterograde movement and retrograde movement were analyzed separately and are shown as the mean±s.e.m.

Cell surface biotinylation studies

To measure the cell surface pool of VEGFR2, we covalently labeled cell-surface proteins using a membrane-impermeant biotinylation reagent (NHS-SS-biotin; Pierce, Rockford, IL) as described previously (Manickam et al., 2011). Total cell proteins and biotinylated surface proteins were analyzed by western blotting using anti-VEGFR2 antibody.

Microtubule dynamics

HUVECs were transfected with EB3 using X-tremeGENE HP (Roche) to visualize microtubule dynamics. Images were acquired every 3 s. Microtubule growth was analyzed using a plusTipTracker software package on 55–65 frames (Matov et al., 2010). Tracking control parameters were as described previously (Komarova et al., 2012). The 'Quadrant Scatter Plot' tool, a part of plusTipTracker package, was used to determine the relationship between growth rate and growth lifetime and to divide microtubules into four subpopulations based on deviation from mean growth speed and growth lifetime (Applegate et al., 2011). The length of microtubule growth from the centrosome was measured using MetaMorph software based on tracks generated with plusTipTracker. The catastrophe frequency was calculated from the number of backward gaps classified as microtubule shrinkage (in contrast to polymer drift during a microtubule pause).

Real-time PCR

Messenger (m)RNA was prepared by using Trizol (Invitrogen) and cDNA was prepared by using reverse transcriptase and oligo dT primer. Real time PCR was performed by using SYBR PCR master mix (ABI, Carlsbad, CA). Primer sets used for real-time PCR were as follows; human VEGFR2 forward, 5′-ATAGAAGGTGCCCAGGAAAAG-3′; reverse, 5′-GTCTTCAGTTCCCCTCCATTG-3′; GAPDH forward, 5′-CAAGGTCATCCATGACAACTTTG; reverse, 5′-GTCCACCACCC-TGTTGCTGTAG-3′.

Transendothelial electrical resistance monitoring of cell migration in real time

Cell migration was measured in real time by using Electric Cell-Substrate Impedance Sensing (ECIS) model 1600R and electrode 8W1E (Applied BioPhysics, Troy, NY) as described previously (Keese et al., 2004).

Scratch wound healing assay

The scratch wound healing assay was performed as described previously (Humtsoe et al., 2010).

Formation of capillary network structures *in vitro*

In vitro capillary network formation on Matrigel (BD Biosciences, San Jose, CA) was performed as described previously (Humtsoe et al., 2010).

In vitro binding analysis

Truncated mutants of KIF13B and VEGFR2 were expressed in BL21 (DE3) or Rosetta-gami and purified as described previously (Yamada et al., 2007). Motor, L1 and DUF2 domains were purified from the soluble fraction. MBS and DUF1 domains were purified from the insoluble fraction using 6 M urea, and re-folded as described previously (Yamada et al., 2007). The binding assay was carried out with S-resin in 0.5% Triton X-100 and 1% BSA at 4℃ and analyzed by western blotting using an anti-GST antibody.

Matrigel plug *in vivo* vessel formation assay

For the Matrigel plug assay to assess vessel formation of mouse cells, C57BL/6 males (Jackson Labs) were used as described previously (Yang and Proweller, 2011). Matrigel supplemented with 4.4 nmol/l VEGF, 50 ng/ml bFGF, 60 U heparin and 0.8×10^8 infectious units of lentivirus was injected subcutaneously into the abdomen. At 4 d after injection, Matrigel was collected. The mice were housed under pathogen-free conditions in the University of Illinois Animal Care facility and treated in accordance with institutional guidelines.

Statistical analysis

Student's *t*-test was used for inter-group comparisons. To analyze more than two samples, one-way ANOVA was used. If the F value was greater than F critical, post-hoc multiple comparisons were performed using GraphPad InStat.

Acknowledgements

We are grateful to Premanand Sundivakkam and Chinnaswamy Tiruppathi for technical advice on the TER assay. We thank Ishita Chatterjee and Norifumi Urao for technical advice regarding the *in vivo* Matrigel plug assay. We thank Anke Di and Varadarajan Sudhahar for kindly providing mouse macrophages and mouse embryonic fibroblasts, respectively. We also thank Haixia Gong for discussions and suggestions concerning this work. We express our gratitude to Scott T. Brady for helpful suggestions. All of those acknowledged here are affiliated with the University of Illinois College of Medicine, Chicago, IL.

Competing interests

The authors declare no competing interests.

Author contributions

K.H.Y. and A.B.M. conceived of and designed the experiments and wrote the paper. K.H.Y. performed all experiments except for those presented in Figs S3C,D and S4C,D. Y.N. performed the experiments presented in Fig. S3C,D. M.G. performed those shown in Fig. S4C,D under supervision of Y.K. Y.K. also supervised quantification of the data presented in Fig. 4B to obtain the graph shown in 4C. K.K.W. supervised the *in vivo* experiments. M.U-F. provided important reagents and helpful discussion.

Funding

This work was supported by grants from National Institutes of Health [grant numbers T32 HL07829 (to A.B.M.), RO1 HL079356 (to K.K.W.), RO1 HL103922 (to Y.K.)]; and a grant from American Heart Association [grant number 13SDG14680053 (to K.H.Y)]. Deposited in PMC for release after 12 months.

Supplementary material

Supplementary material available online at http://jcs.biologists.org/lookup/suppl/doi:10.1242/jcs.156109/-/DC1

References

Applegate, K. T., Besson, S., Matov, A., Bagonis, M. H., Jaqaman, K. and Danuser, G. (2011). plusTipTracker: quantitative image analysis software for the measurement of microtubule dynamics. *J. Struct. Biol.* **176**, 168-184.

Bruns, A. F., Bao, L., Walker, J. H. and Ponnambalam, S. (2009). VEGF-A-stimulated signalling in endothelial cells via a dual receptor tyrosine kinase system is dependent on co-ordinated trafficking and proteolysis. *Biochem. Soc. Trans.* **37**, 1193-1197.

Di, A., Gao, X. P., Qian, F., Kawamura, T., Han, J., Hecquet, C., Ye, R. D., Vogel, S. M. and Malik, A. B. (2011). The redox-sensitive cation channel TRPM2 modulates phagocyte ROS production and inflammation. *Nat. Immunol.* **13**, 29-34.
Domingues, I., Rino, J., Demmers, J. A., de Lanerolle, P. and Santos, S. C. (2011). VEGFR2 translocates to the nucleus to regulate its own transcription. *PLoS ONE* **6**, e25668.
Eskelinen, E. L., Tanaka, Y. and Saftig, P. (2003). At the acidic edge: emerging functions for lysosomal membrane proteins. *Trends Cell Biol.* **13**, 137-145.
Ewan, L. C., Jopling, H. M., Jia, H., Mittar, S., Bagherzadeh, A., Howell, G. J., Walker, J. H., Zachary, I. C. and Ponnambalam, S. (2006). Intrinsic tyrosine kinase activity is required for vascular endothelial growth factor receptor 2 ubiquitination, sorting and degradation in endothelial cells. *Traffic* **7**, 1270-1282.
Ferrara, N. (2009). Vascular endothelial growth factor. *Arterioscler. Thromb. Vasc. Biol.* **29**, 789-791.
Folkman, J. (2007). Angiogenesis: an organizing principle for drug discovery? *Nat. Rev. Drug Discov.* **6**, 273-286.
Gampel, A., Moss, L., Jones, M. C., Brunton, V., Norman, J. C. and Mellor, H. (2006). VEGF regulates the mobilization of VEGFR2/KDR from an intracellular endothelial storage compartment. *Blood* **108**, 2624-2631.
Graupera, M., Guillermet-Guibert, J., Foukas, L. C., Phng, L. K., Cain, R. J., Salpekar, A., Pearce, W., Meek, S., Millan, J., Cutillas, P. R. et al. (2008). Angiogenesis selectively requires the p110alpha isoform of PI3K to control endothelial cell migration. *Nature* **453**, 662-666.
Hanada, T., Lin, L., Tibaldi, E. V., Reinherz, E. L. and Chishti, A. H. (2000). GAKIN, a novel kinesin-like protein associates with the human homologue of the Drosophila discs large tumor suppressor in T lymphocytes. *J. Biol. Chem.* **275**, 28774-28784.
Herbert, S. P. and Stainier, D. Y. (2011). Molecular control of endothelial cell behaviour during blood vessel morphogenesis. *Nat. Rev. Mol. Cell Biol.* **12**, 551-564.
Hirokawa, N., Noda, Y., Tanaka, Y. and Niwa, S. (2009). Kinesin superfamily motor proteins and intracellular transport. *Nat. Rev. Mol. Cell Biol.* **10**, 682-696.
Horiguchi, K., Hanada, T., Fukui, Y. and Chishti, A. H. (2006). Transport of PIP3 by GAKIN, a kinesin-3 family protein, regulates neuronal cell polarity. *J. Cell Biol.* **174**, 425-436.
Humtsoe, J. O., Liu, M., Malik, A. B. and Wary, K. K. (2010). Lipid phosphate phosphatase 3 stabilization of beta-catenin induces endothelial cell migration and formation of branching point structures. *Mol. Cell. Biol.* **30**, 1593-1606.
Itoh, S., Kim, H. W., Nakagawa, O., Ozumi, K., Lessner, S. M., Aoki, H., Akram, K., McKinney, R. D., Ushio-Fukai, M. and Fukai, T. (2008). Novel role of antioxidant-1 (Atox1) as a copper-dependent transcription factor involved in cell proliferation. *J. Biol. Chem.* **283**, 9157-9167.
Keese, C. R., Wegener, J., Walker, S. R. and Giaever, I. (2004). Electrical wound-healing assay for cells in vitro. *Proc. Natl. Acad. Sci. USA* **101**, 1554-1559.
Komarova, Y. A., Huang, F., Geyer, M., Daneshjou, N., Garcia, A., Idalino, L., Kreutz, B., Mehta, D. and Malik, A. B. (2012). VE-cadherin signaling induces EB3 phosphorylation to suppress microtubule growth and assemble adherens junctions. *Mol. Cell* **48**, 914-925.
Lanahan, A. A., Hermans, K., Claes, F., Kerley-Hamilton, J. S., Zhuang, Z. W., Giordano, F. J., Carmeliet, P. and Simons, M. (2010). VEGF receptor 2 endocytic trafficking regulates arterial morphogenesis. *Dev. Cell* **18**, 713-724.
Manickam, V., Tiwari, A., Jung, J. J., Bhattacharya, R., Goel, A., Mukhopadhyay, D. and Choudhury, A. (2011). Regulation of vascular endothelial growth factor receptor 2 trafficking and angiogenesis by Golgi localized t-SNARE syntaxin 6. *Blood* **117**, 1425-1435.
Matov, A., Applegate, K., Kumar, P., Thoma, C., Krek, W., Danuser, G. and Wittmann, T. (2010). Analysis of microtubule dynamic instability using a plus-end growth marker. *Nat. Methods* **7**, 761-768.
Matsumoto, T. and Claesson-Welsh, L. (2001). VEGF receptor signal transduction. *Sci. STKE* **2001**, re21.
Morfini, G. A., Burns, M., Binder, L. I., Kanaan, N. M., LaPointe, N., Bosco, D. A., Brown, R. H., Jr, Brown, H., Tiwari, A., Hayward, L. et al. (2009). Axonal transport defects in neurodegenerative diseases. *J. Neurosci.* **29**, 12776-12786.
Nagy, J. A., Dvorak, A. M. and Dvorak, H. F. (2007). VEGF-A and the induction of pathological angiogenesis. *Annu. Rev. Pathol.* **2**, 251-275.
Nakatsu, M. N. and Hughes, C. C. (2008). An optimized three-dimensional in vitro model for the analysis of angiogenesis. *Methods Enzymol.* **443**, 65-82.
Nakayama, M., Nakayama, A., van Lessen, M., Yamamoto, H., Hoffmann, S., Drexler, H. C., Itoh, N., Hirose, T., Breier, G., Vestweber, D. et al. (2013). Spatial regulation of VEGF receptor endocytosis in angiogenesis. *Nat. Cell Biol.* **15**, 249-260.
Newman, A. C., Nakatsu, M. N., Chou, W., Gershon, P. D. and Hughes, C. C. (2011). The requirement for fibroblasts in angiogenesis: fibroblast-derived matrix proteins are essential for endothelial cell lumen formation. *Mol. Biol. Cell* **22**, 3791-3800.
Potente, M., Gerhardt, H. and Carmeliet, P. (2011). Basic and therapeutic aspects of angiogenesis. *Cell* **146**, 873-887.
Rahimi, N. (2009). A role for protein ubiquitination in VEGFR-2 signalling and angiogenesis. *Biochem. Soc. Trans.* **37**, 1189-1192.
Saharinen, P., Eklund, L., Pulkki, K., Bono, P. and Alitalo, K. (2011). VEGF and angiopoietin signaling in tumor angiogenesis and metastasis. *Trends Mol. Med.* **17**, 347-362.
Sakurai, Y., Ohgimoto, K., Kataoka, Y., Yoshida, N. and Shibuya, M. (2005). Essential role of Flk-1 (VEGF receptor 2) tyrosine residue 1173 in vasculogenesis in mice. *Proc. Natl. Acad. Sci. USA* **102**, 1076-1081.
Shibuya, M. and Claesson-Welsh, L. (2006). Signal transduction by VEGF receptors in regulation of angiogenesis and lymphangiogenesis. *Exp. Cell Res.* **312**, 549-560.
Singh, A. J., Meyer, R. D., Navruzbekov, G., Shelke, R., Duan, L., Band, H., Leeman, S. E. and Rahimi, N. (2007). A critical role for the E3-ligase activity of c-Cbl in VEGFR-2-mediated PLCgamma1 activation and angiogenesis. *Proc. Natl. Acad. Sci. USA* **104**, 5413-5418.
Verhey, K. J., Lizotte, D. L., Abramson, T., Barenboim, L., Schnapp, B. J. and Rapoport, T. A. (1998). Light chain-dependent regulation of Kinesin's interaction with microtubules. *J. Cell Biol.* **143**, 1053-1066.
Yamada, K. H., Hanada, T. and Chishti, A. H. (2007). The effector domain of human Dlg tumor suppressor acts as a switch that relieves autoinhibition of kinesin-3 motor GAKIN/KIF13B. *Biochemistry* **46**, 10039-10045.
Yang, K. and Proweller, A. (2011). Vascular smooth muscle Notch signals regulate endothelial cell sensitivity to angiogenic stimulation. *J. Biol. Chem.* **286**, 13741-13753.
Zhang, X., Goncalves, R. and Mosser, D. M. (2008). The isolation and characterization of murine macrophages. *Current Protoc. Immunol.* **Chapter 14**, Unit 14.11.